Seasonal and co-seismic velocity variation in the region of L'Aquila from single station 1 measurements and implications for crustal rheology 2 3 AUTHORS

Piero Poli, Valenting Marguin, Qingyu Wang, Nicola d'Agostino, Paul A. Johnson

▶ **To cite this version:**

Seasonal and co-seismic velocity variation in the region of L'Aquila from single station measurements and implications for crustal rheology

AUTHORS: *Piero Poli[1], Valenting Marguin[2], Qingyu Wang[1], Nicola D'Agostino[3], Paul Johnson[4]*

1- *Institut de Sciences de la Terre,* Université Grenoble Alpes, CNRS (UMR5275), Grenoble, France.
2- Département des sciences de la Terre, Université de Genève, 1205 Geneva, Switzerland
3- *Osservatorio Nazionale Terremoti, Istituto Nazionale Geofisica Vulcanologia, Roma, Italy*
4- *Geophysics, Los Alamos National Laboratory, Los Alamos, New Mexico USA 87545*

ABSTRACT

We performed time lapse measurements of velocity variations using empirical Green's functions reconstructed by autocorrelation of seismic noise recorded during a period of 17 years in the region of l'Aquila, Italy. The time lapse approach permitted us to evaluate the spatial (depth) dependence of velocity variation (dv/v). By quantitatively comparing the 17 years of dv/v time series with independent data (e.g. strain induced by earthquakes, hydrological loading) we unravel a group of physical processes inducing velocity variations in the crust over multiple time and spatial scales. We find that rapid shaking due to three magnitude 6+ earthquakes mainly induced near surface velocity variations. On the other hand, Slow strain perturbation (period 5 years) associated with hydrological cycles, induced velocity changes primarily in the middle-crust. The observed behavior suggests the existence of a large volume of fluid filled cracks exist deep in the crust. Our study, beyond shedding new light into the depth dependent rheology of crustal rocks in the region or l'Aquila, highlights the possibility of using seasonal and multiyear perturbations to probe the physical properties of seismogenic fault volumes.

1. Introduction

Detailed laboratory protocols exist to estimate how rocks respond to strain perturbations, and show that a variety of non-linear responses exists for variable rock types with different physical properties (e.g. cracks density, microstructure, presence of fluid, temperature and pressure effects—Guyer & Johnson, 1999;2009; Ostrovsky and Johnson, 2001; Renaud et al., 2009, 2012, Riviere et al., 2015).

One approach to describing nonlinear elastic and plastic properties of rock is applying 'effective viscosity' (e.g. Lyakhovsky et al., 2001, Ben-Zion, 2008). Numerical simulations (Lyakhovsky et al., 2001, Hamiel et al., 2006; Lott et al.2018) show how this effective parameter plays a fundamental role in how rocks respond to strain perturbation, and thus controls phenomena occurring during the seismic cycle (e.g. clustering of seismicity, foreshocks, style of nucleation, amount of aseismic slip). The effective viscosity parameter has similarities to the hysteretic nonlinear parameter in the Priesach-Mayergoyz description of elasticity (McCall and Guyer 1993; Guyer and Johnson 2009). The latter has a direct link with damage intensity (e.g., Guyer and Johnson 1999; Johnson 1998, Van Den Abeele and Visscher, 2000, Ostrovsky and Johnson 2001). Other models that describe these behaviours, as well including Ahrennius approaches for hysteresis, exists (e.g., Ostrovsky et al., 2019; Sens-Schoenfelder et al., 2018).

It is thus fundamental to characterize the physical properties of rocks surrounding seismogenic faults, to better understand the role of rheology and elasticity during the

seismic cycle, and associated phenomena that can arise in fault(s). Field observations emulating laboratory protocols have been attempted, by studying velocity variations due to strong, surface active-source induced shaking (e.g., Johnson et al., 2009), as well as rocks subjected to cycles of tidal forcing and induced seismicity (e.g., Delorey et al, 2017; van der Elst et al, 2017 and active seismic experiments probing the effects of Earth tides (e.g. Yamaura et al., 2003). More recently, the ability of estimating the Green's function from seismic noise (Shapiro & Campillo, 2004), has made it possible to monitor velocity variations (e.g. Brenguier et al., 2014) without the need of active sources (e.g. explosions; vibrators), and more recent studies applied this method to study the response of rocks to tidal strain (Takano et al., 2014, Hillers et al., 2015b). However, at present only the shallowest portions of the crust (primarily less than 1km of depth) have been explored (Takano et al., 2014, Hillers et al., 2015b) and at most, depths to 5 km, following the 2004 M6.0 Parkfield earthquake (Wu et al., 2017), thus permitting the characterization of shallow damage zones, but not deeper regions, where the most seismicity occurs and large earthquakes nucleate (see Ben-Zion, 2008, and reference therein).

It has been demonstrated that detailed lapse-time monitoring applying coda waves reconstructed from correlation of seismic noise can provide important information about the deeper part of the crust (Obermann et al., 2013, Obermann et al., 2014, Hillers et al., 2018). These results have been validated with numerical experiments, providing clues regarding the depth resolution of velocity variation (dv/v) as function of coda lapse-time (Obermann et al., 2013).

In this work, we performed time lapse monitoring of dv/v near to the city of L'Aquila, in the central Apennines (Italy). This region is characterized by active normal faulting that accommodates the ongoing ~3 mm/yr tectonic extension (D'Agostino, 2014, Fig. 1). As a result, normal faults capable of producing magnitude 6+ events are present along the entire Apennine chain. The region of L'Aquila itself is characterized by significant seismic hazard, and was recently struck by 3 magnitude 6+ earthquakes (http://iside.rm.ingv.it, Fig. 1).

We here estimate the spatial (depth) response (dv/v) of the medium to periodic perturbations. Instead of relying of tidal strain as has been applied by others (e.g., Hillers et al., 2015), we exploit periodic perturbations associated with multiyear-long hydrological cycle related to the recharge of karst aquifers (e.g. Silverii et al., 2019). These perturbations provide significant strain at the surface (relative baseline elongation up to 10-6 mm within few tens of kilometers, mostly horizontal) with poorly resolved extension at depth. Correlation with seismicity rate in the 1.2-3.9 magnitude range in the southern Apennines (D'Agostino et al., 2019) suggests that stress perturbations induced by the hydrological forcing may extend to a depth larger than 5 km and thus affect the seismogenic portion of the crust (Fig. 1). In particular, we assess how dv/v over different time windows, evolves for episodes of dilatation and compression of the crust (Silverii et al., 2019). We further estimate the response of the medium to earthquakes (M>6) that occurred during the study period (2000-2016).

In the following, we begin by describing the procedures to derive estimates of the Green's function and measure velocity variations (sec. 2). We then analyze evolution of dv/v for periodic perturbation and during coseismic periods (sec. 3 and 4). Finally, we discuss the results and the peculiar evolution of dv/v as a function of lapse-time that we observed (sec. 5). Our results suggest that an isolated region extended into the middle-lower crust is particularly sensitive to deformations. We interpret this observation as due to the presence of significant amounts of fluid filled cracks at depth that make the material more susceptible to the nonlinear elastic changes we observe.

2. Seismic noise correlation and time lapse velocity variation

a. Estimation of the Green's function from noise correlation

We calculate the three-component (ZZ, EE, NN) autocorrelation using continuous seismic data recorded at the AQU station located in central Italy (Fig. 1). We focus on the time period from January 1 2000 to December 31 2017 (17 years). Each daily trace of seismic data is split in 10min windows with 50% overlap, after the deconvolution of the instrumental response and filtering between 0.5 and 1Hz. After analyzing several frequency bands, we choose to focus on 0.5-1Hz range as it provides the highest quality correlation, while limiting the amount of stacked days, thus increasing the time resolution of our analysis.

To remove spurious spikes and contributions from earthquakes, we calculate the sum of the squared signal (energy) for each window, and remove those exceeding the daily mean of the energy plus 3 standard deviations (Poli et al., 2012). We ensure that, after this test, at least 20 hours of data are still contained in the daily trace; otherwise the daily trace is rejected. The time windows passing the amplitude test are one-bit normalized to further reduce transient signals (e.g. earthquakes), which may escape our processing.
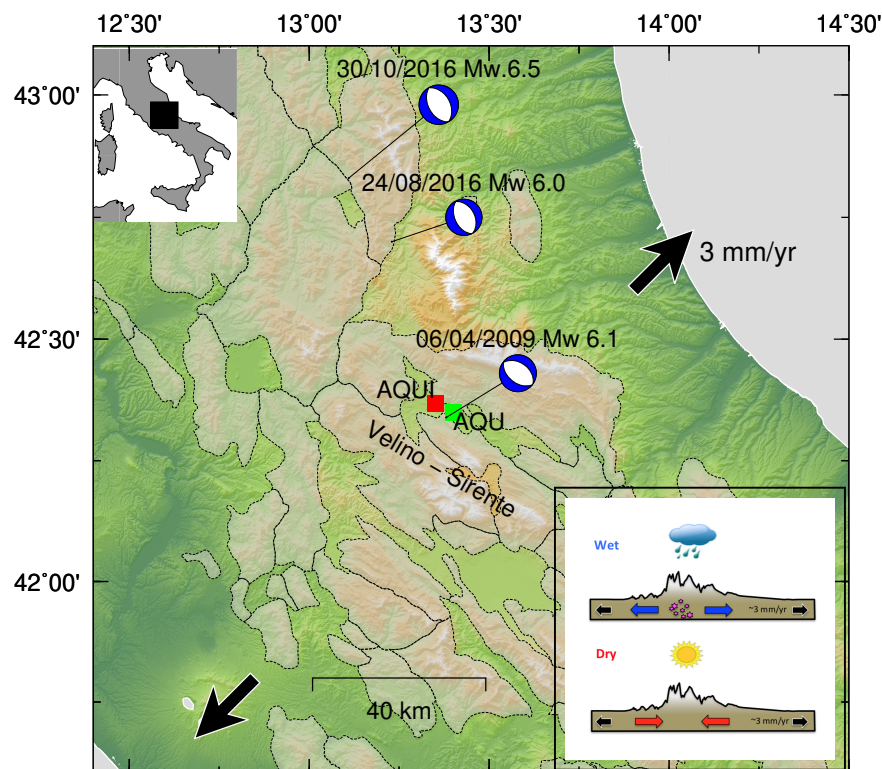
Figure 1. *Map of the study area. The upper inset shows the location of the study area in Italy. The squares indicate the location of the seismic (AQU, in green) and GPS (AQUI, in red) stations. Beach balls show focal mechanism of the main events from 2009 to 2016 (from Scognamiglio et al., 2006). Shaded areas include regions where carbonate lithologies host large karst aquifers (see Silverii et al., 2019). The lower inset shows a conceptual drawing of the modulation of crustal deformation and seismicity by seasonal and multi-annual recharge/discharge phases of of karst aquifers.*

b. Measurement of velocity variation (dv/v)

We measure the velocity variations using both stretching (Lobkis & Weaver, 2003) and doublet (Poupinet et al., 1984) techniques. While the two methods provide similar results (Fig. S3), additional tests have shown that the stretching technique provides less noisy measurements, and therefore will be used here.

In detail, the velocities are obtained by stacking 90 days using a 89 day overlap of correlations, to ensure stable dv/v measures (Sabra et al., 2005). Each stacked correlation is then compared, using the methods mentioned above, with a reference signal (the stack of the correlation over the full-time period) to estimate the dv/v over different coda waves lapse-time (table 1). We then average the dv/v over different components, weighting with squared correlation coefficients estimated after stretching. Only signals with correlation larger than 0.9 are retained, and a stack is performed if all the 3 components are available.

c. Lapse time and depth sensitivity of dv/v

In this section, we estimate the first order depth resolution for our velocity variation measures. It should be kept in mind however, that the sensitivity to absolute depth requires detailed measures of the scattering properties of the medium, which are not available for the study area (Obermann et al. 2013; 2016, Kanu and Snieder, 2015). Nevertheless, we can reason around existing theoretical and numerical results to gain insights about relative depth resolution of coda waves measured at different lapse time of the coda (Obermann et al. 2013; 2016, Kanu and Snieder, 2015).

Despite the depth sensitivity of coda waves has not been fully quantitatively solved yet, it is well known that the sensitivity to dv/v in a medium varies with frequency and time lapse of the coda waves used (i.e., deeper sampling for larger lapse-time) (e.g. Pacheco & Snieder, 2005, Obermann et al., 2013, Wu et al., 2017). Numerical simulations (Obermann et al. 2013, 2016) reported that the sensitivity of coda waves is due to a combination of the sensitivities of body waves and surfaces waves. In the early normalized lapse-time, t less than ~ 6 (t is normalized by mean free time t*), the coda wave sensitivity is controlled by the surface wave sensitivity. With increasing lapse-time, the body wave sensitivity becomes progressively more important.

We thus start by estimating the sensitivity of surface waves (Hermann, 2013), using a local velocity model (Chiaraluce et al., 2009) and a frequency of 0.75Hz (Fig. 2b). The resulting surface wave kernel suggest sensitivity in the uppermost 4km of the crust.

We furthermore evaluate the sensitivity of the scattered body waves by considering a 3-D sensitivity kernel formulation by Pacheco and Snieder (2005). The energy propagator p is calculated by the radiative transfer solution approximation for isotropic scattering (Paasschens, 1997; Planès et al., 2014). We estimate the theoretical depth sensitivities of the body wave velocity changes with scattering mean free paths from 10 km and 100 km, proxies for the high and low frequency regimes (Lacombe et al., 2003, Hiller at al., 2019). The energy velocity is determined by the equipartition state. We take the theoretical equipartition ratio as 10.4 and 3 for a Poisson solid (Margerin et al., 2000; Weaver, 1982), the same as Wang et al. (2019), for further calculation. We solved for the body wave depth sensitivity normalized to 30 km depth with each layer 1 km thick layer.

Figure 2a gives the calculated normalized body wave kernel. The calculation follows the details described by Obermann et al., (2013), Planès et al. (2014), Obermann et al. (2016), and Wang at al., (2019). We clearly observe that using the mean free path (l) equal to 100 km (low frequency regime), the depth sensitivity is deeper than using the smaller mean free path l as 10 km. This is an indication of the frequency-dependent depth
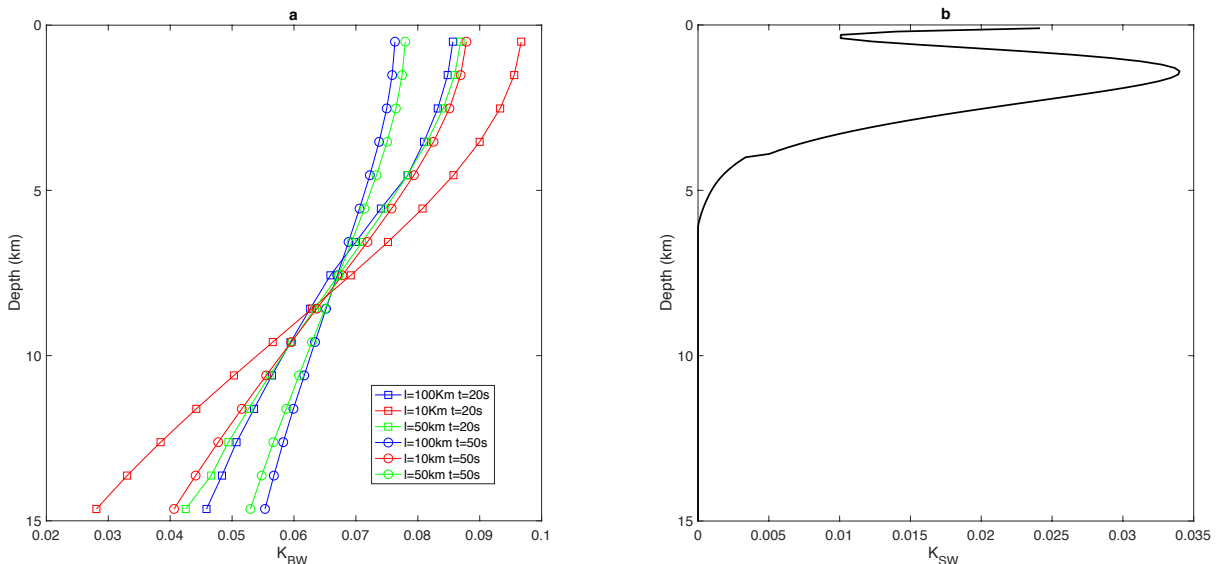
181   sensitivity of body waves, which is the same characteristic surface waves exhibit (Fig. 2a).
182   We also observe how the depth sensitivity increases gradually as the lapse-time becomes
183   progressively larger from 20 s to 50 s with the same mean free path. Thus, we measure the
184   seismic velocity changes for deeper strata applying later lapse-times (Fig. 2a). This result,
185   suggest that by observing the time-lapse evolution of dv/v across the coda, we can get
186   insights about velocity variation into deep layers. A similar conclusion was draw by
187   Obermann et al. (2013) by using numerical modeling.
188   Guided by the calculated kernels and results from previous studies (Obermann et al.
189   2013), we defined a set of windows (table 1) to scan different depths of the crust, similarly
190   to previous studies based on autocorrelation (e.g. Ricther et al., 2014). In more detail, we
191   defined 3 starting times (10, 20, and 30s) after zero time (ballistic waves arrival time). For
192   each starting time, we vary the length of the time window to perform stretching (20, 40,
193   60s). The goal of this coda lapse-time dependent analysis is to resolve any evolution of
194   dv/v, which can reveal the linear and nonlinear elastic response as function of relative depth
195   (e.g. increment of dv/v with coda lapse time will highlight larger velocity changes at depth).
196

197   ***Table 1:*** *Time lapse for calculation of dv/v.*

Window number	Time start (s)	Time end (s)
1	*10*	*30*
2	*10*	*50*
3	*10*	*70*
4	*20*	*40*
5	*20*	*60*
6	*20*	*80*
7	*30*	*50*
8	*30*	*70*
9	*30*	*90*

198
199

201   ***Figure 2:*** *a) Body waves sensitivity kernels for variable mean free paths lapse-times.*
202   *b) Surface waves sensitivity kernel.*

203
204   ***d.   Comparison of dv/v with other estimates***

205   The velocity variation (dv/v) time series for window 4 (20s to 40s lag time) is shown
206 in figure 3 (measures for the other time lapse intervals are shown in figures 4 and 7, for
207 periodic and co-seismic perturbations respectively). Two primary velocity decreases are
208 observed. The largest decrease (relative dv/v~0.3%) is associated with the occurrence of
209 the magnitude 6.3 L'Aquila earthquake (iside.rm.ingv.it). The second decrease (relative
210 dv/v ~0.15%) occurred in 2016 during the Norcia-Visso seismic sequence (Chiaraluce et
211 al., 2016), which includes 2 M6+ earthquakes. Besides of these major coseismic drops, we
212 observe cyclic variations of dv/v up to 0.05% (fig. 3b).
213   Silverii et al. (2016, 2019) analyzed GPS data in the study region, showing the presence
214 of transient deformations associated with multiyear hydrological cycles (~5yrs). During
215 these cycles the crust undergoes significant extension and compression (up to 3mm/yr)
216 sustained for 2-3 years associated, respectively, with phases of recharge and discharge of
217 karst aquifers that modulate the secular, tectonic strain accumulation (see inset Fig. 1).
218 These cycles are visible in both the rain time series (shown as detrended cumulative rain in
219 fig. 3c) and in the detrended horizontal GPS motion (fig. 3e) recorded at the station AQUI
220 (fig. 1). Here we use the east-component time series of the AQUI site corrected for long-
221 term trend and instrumental offsets (see Silverii et al., 2019 for details of the processing).
222   In periods of significant aquifer recharge (e.g. 2005 to 2007) the AQUI site is subject
223 to a significant eastward displacement (~5mm), while the opposite motion is recorded for
224 dry periods. As reported by Silverii et al (2019) the multi-seasonal, hydrological forcing
225 associated to the recharge of karst aquifers induces a measurable surface deformation up to
226 ~90 nanostrain/yr. The AQUI station is mostly sensitive to the large Velino-Sirente karst
227 system (Fig. 1) alternatively moving to the north-east during phases of high recharge and
228 to the south-west during phases of low-recharge (Silverii et al., 2019). This motion is
229 superimposed on the steady SW-NE 3 mm/yr extension across the Apennines. It is
230 important to note that this phenomenon is pervasively observed along the Apennines at
231 stations located close to main karst aquifers (Silverii et al., 2016, 2019; D'Agostino et al.,
232 2018).
233   Similarly, and in agreement with previous studies (e.g. Hillers et al., 2015a, Wang et
234 al. 2017), the dv/v follows the hydrological cycle, with a velocity drop for increasing
235 hydraulic head and vice versa. The dv/v also shows shorter term oscillations (~1yr) which
236 are visually correlated with the variation of surface temperature (fig. 3d). In agreement with
237 previous studies (e.g. Richter et al., 2014) a decrease in temperature coincides with a
238 reduction of dv/v. Alternatively, these, short-term oscillations can be due to short term
239 seasonal hydrological effects similar to what is observed in the GPS time series (Silverii et
240 al., 2016).
241   In the remainder of this work we will quantify the response of the crust to periodic
242 (hydrological) and tectonic (earthquakes) forcing and assess the sensitivity of different
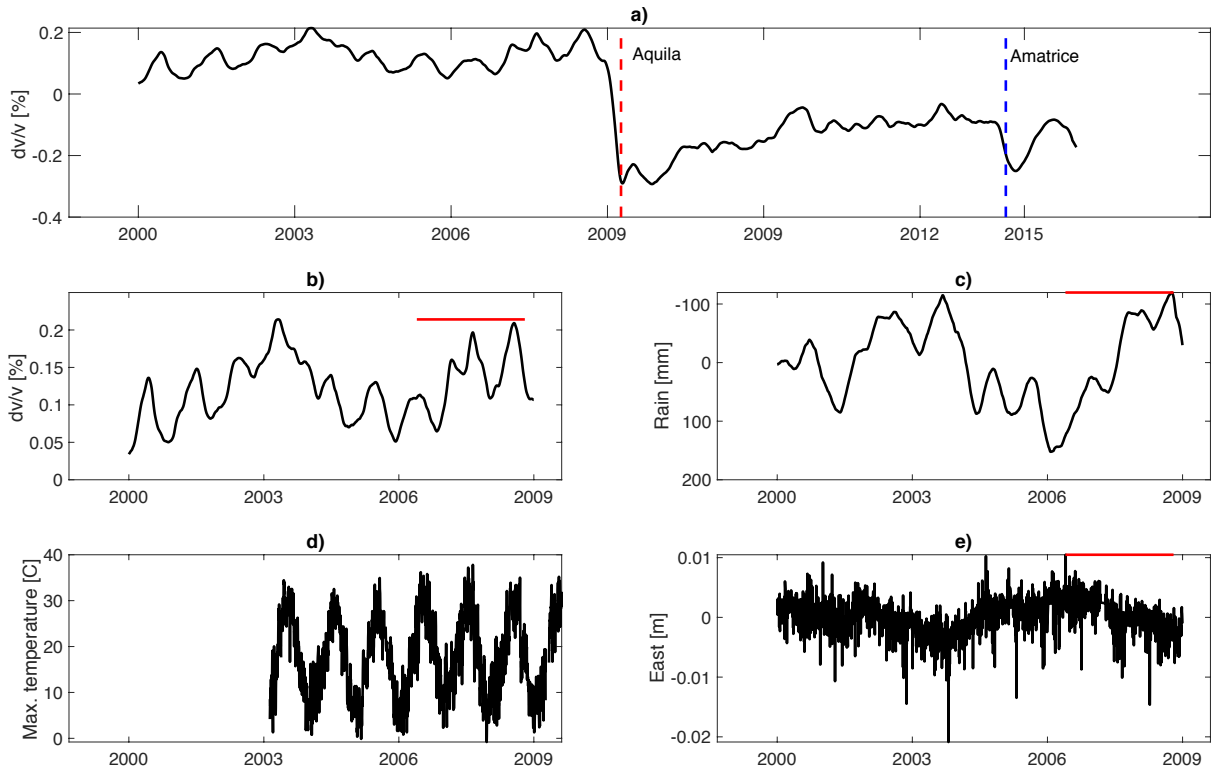243 crustal levels to these deformations.
244
245

FIGURE 3: *Summary of observations in the study area. a) Time series of velocity variation for the entire period, with major earthquakes highlighted. b) dv/v time series during the preseismic period. c) Detrended cumulative rain as in Silverii et al. (2019) (y-axis is inverted). d) Daily maximum temperature. e) East GPS displacement at station AQUI corrected for tectonic trend and antenna offset from Silverii et al.(2009). The red solid line indicate a dry period identified by Silverii et al.(2009).*

3. *Sensitivity to cyclic deformations and probing the mid-crust*

a. *Decomposition of dv/v time series*

We quantitatively evaluate the seasonal and multi-years components of dv/v estimated for different lapse times (see table 1). In this section, we focus only on the pre-seismic period, using dv/v measured before L'Aquila earthquake (beginning of 2000 to end of 2008).

We start by modeling the relative contribution of the multiyear and seasonal effect on dv/v with a phenomenological model (e.g. Taira et al, 2018):

$$\frac{dv}{v}_S = A + B\cos\left(\frac{2\pi}{C*365}(t - D)\right) + E\cos\left(\frac{2\pi}{F*365}(t - G)\right) [2]$$

In eq. 2, A is a global offset, B and E are the amplitudes of the two modelled cycles, C and F are the cycle duration in years, while D ang G account for the cosine phase shift. We fit all dv/v time series using a non-linear least squares approach. From the inversion, we find that for all selected time lapses the best-fit durations of the cycles are C=1±0.02yr and F=5±0.1yrs.

The results of our fits are shown in figure 4 (red and green lines) together with the original data (blue lines). It can be observed that while the dv/v amplitude of seasonal 1-yr oscillation (B) is higher at earlier lapse times, progressive decreases in the later coda are observed where dv/v is more sensitive to the 5yr cycle (E). To better

visualize the results, we plot in figure 5 the B and E terms of equation 2 as function of coda lapse time. While the amplitude of the short-term cycle decreases at larger lapse time, the opposite behavior is observed for the amplitude of the 5-yrs (E). The ratio of the B and E parameters (fig. 5b) suggests that beyond 20s lapse time dv/v is dominated by the long-term cycle.
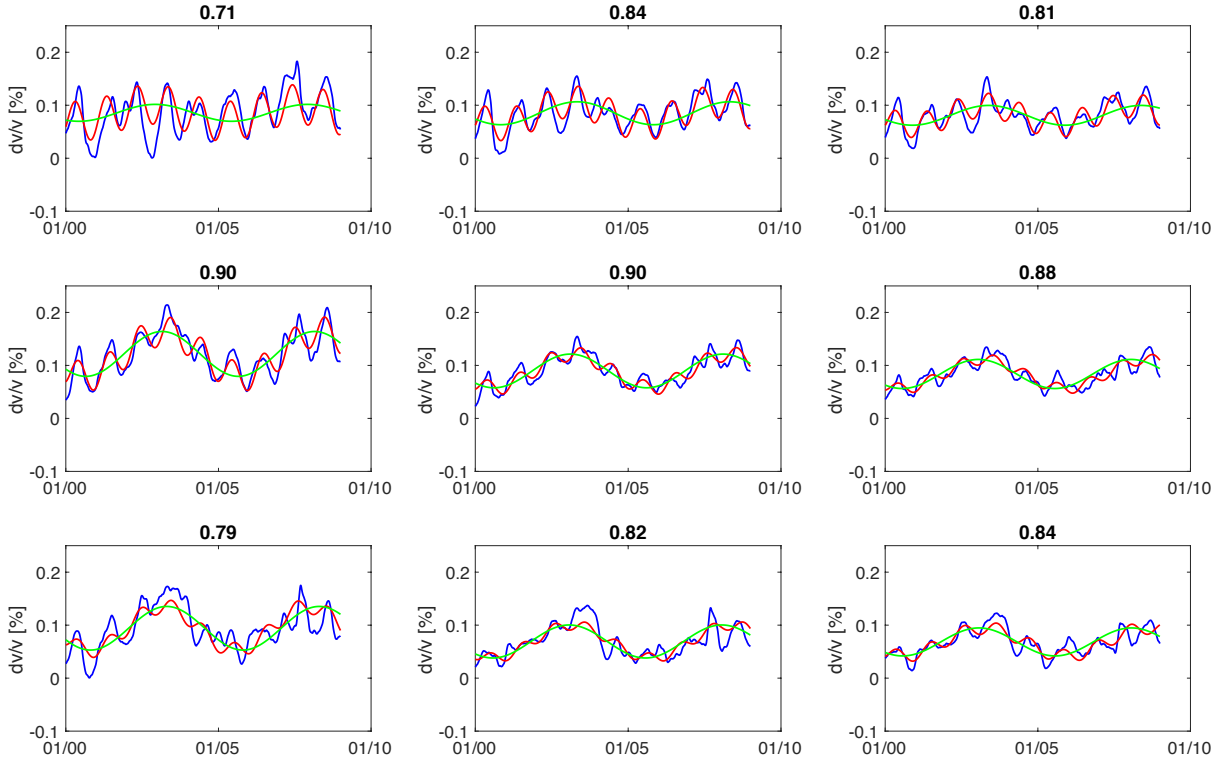
Figure 4: *dv/v (blue) and modeled cycles with eq. 2 (red) for coda windows reported in table 1. The green line represents the long-term portion (first and third righthand terms of eq. 1). Numbers on top of each plot are the correlation coefficient between the model (eq. 2, red) and the data (blue).*

The decay of the parameter B (fig. 3a) and the B/E ratio (fig. 3b), suggests that the source of the 1yr periodicity in dv/v is dominantly at shallow depths (Obermann et al., 2013, see also the kernels in fig. 2). It has been suggested that thermally induced stresses rapidly decays with depth (Ben-Zion & Leary, 1986), and the effects on dv/v have been reported in other regions (e.g. Richter et al, 2014). Thus, as the short-term cycle closely follows the seasonal temperature variation (fig. 3d, see fig S1) and shows a rapid decay as a function of depth, we infer that temperature plays a primary role in controlling the dv/v.
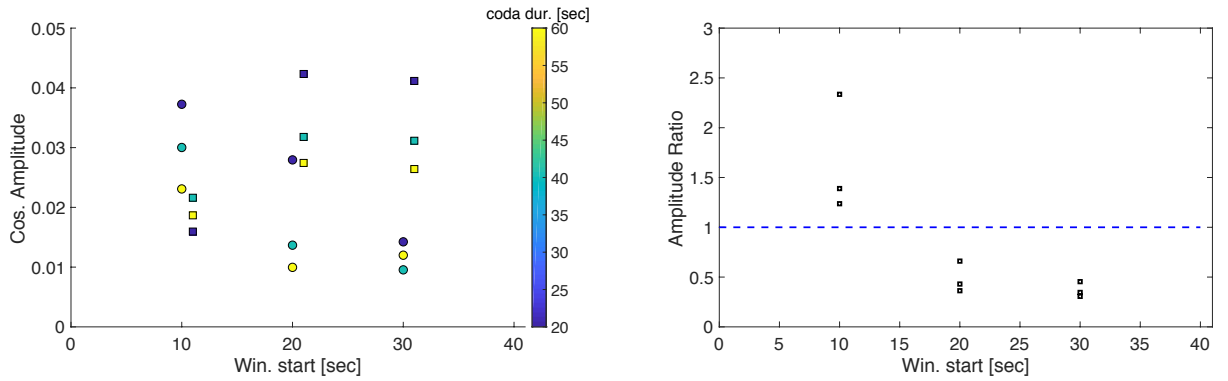
Figure 5: *Magnitude of B (round) and E (squares) as function of coda window time (left). The color indicates the duration of the window. Squares are offset by 1sec for clarity. Ratio B/E as function of coda window order (right, black).*

The long period oscillations of dv/v are strongly correlated with the long-term variation of rainfall (fig. 3c) and GPS deformation (fig. 3e, S2). This multiyear signal represents transient deformations, occurring in highly fractured crustal rock as a response to variations of the hydraulic head in karst aquifers, and induces a strain rate up to ~90 nanostrain/yr (Silverii et al., 2019). This strain rate temporarily increases during high recharge, or diminishes during droughts, and can locally exceed the long-term secular tectonic strain rate (D'Agostino, 2014). The dv/v for later lapse times better correlates with this long period deformation (fig. 5). This observation suggests that a particular depth of the crust is more susceptible to these periodic perturbations (Obermann et al., 2013). Furthermore, we observe how for these late lapse-times (or depths) the short-term cycle has limited effect (2 to 4 times smaller, Fig. 5). As the thermally induced stress rapidly decays with depth (Ben-Zion & Leary, 1986), we can further confirm that the late coda evolution of dv/v is sensitive to deeper layers.

b. *Probing the crust with long term (5yrs) periodic deformations*

We probe the rheological response of the crust to these perturbations using time lapse measures of dv/v, similar to what has been done in other regions with tidal strain (Takano et al., 2014, Hillers et al., 2015b). To reiterate, the goal is to derive a lapse time (or depth) dependent measurements of dv/v representative of perturbations at different crustal levels in order to reveal physical properties of rocks at different depth (e.g. Obermann et al., 2015, Hillers et al., 2018).

The *in-situ* measurements resemble laboratory dynamic acoustoelastic testing, a 'pump-probe' method (e.g., Renaud et al., 2009, 2012). Here, the medium changes are evaluated by estimating dv/v using the reconstructed Green's function (the 'probe'), while the medium is deformed by long period (~5yrs) perturbations (the 'pump') shown by the GPS signal (Silverii et al., 2019, Fig. 2). More precisely, we create a new set of autocorrelations by stacking 300 days of data with 200 days overlap. This time windowing helps us to reduce the short-term fluctuations (1yr). For each time segment dv/v is estimated by comparing the estimated Green's function, with a reference signal from stacking over the full period (2000 to end of 2008). We use the stretching method and the same coda time windows listed in table 1. The deformation is obtained from the projection of the east and north components of the GPS time series recorded at the AQUI station (Fig. 1), along the N45 direction, to maximize the amplitude of the hydrologically-related deformation ($\hat{d}$) (Silverii et al., 2019). The GPS time series is indicative for the strain in the crust (Silverii et al., 2019): negative (south-westward) $\hat{d}$

338 correspond to horizontal contraction, whereas positive $\hat{d}$ (north-eastward) values are
339 representative of horizontal dilatation.
340   We then infer the sensitivity of dv/v to deformation in each time window by
341 fitting the data (fig. 6) with a linear model:

342

343
$$\frac{\delta v}{v} = \alpha + \beta \hat{d} \quad [3]$$

344

345   Equation 3 is similar to strain-dv/v relationship used to study the sensitivity to
346 tidal strain (Takano et al., 2014, Hillers et al., 2015b), where β represents the sensitivity
347 to deformation while the zero-offset is α. Our phenomenological model can be
348 compared to the 1-D non-linear elasticity equation derived in Landau and Lifshutz
349 (2012) and broadly applied to Earth materials (e.g., Guyer and Johnson, 1999;2009).
350 We can interpret the sensitivity to elastic deformation (β) as the classic non-linear
351 elastic parameter that describes the slope of $\delta v/v$ over a single low frequency pump
352 cycle. α is the non-linear volumetric change (length change in 1D) related to material
353 conditioning (Guyer & Johnson, 2009). Note in eq. 3 we do not include the cubic non-
354 linear elastic parameter that describes curvature in $\delta v/v$ as the scattering in the data
355 provide similar misfit for 1st and 2nd order polynomial fit, nor the hysteretic term that is
356 common to Earth materials.
357   The results in figure 6 show that, in agreement with experimental observations
358 in laboratory rock samples (e.g. Renaud et al., 2012), velocity increases under
359 compression (negative $\hat{d}$) and reduces during expansion episodes (positive $\hat{d}$). Similar
360 results have been obtained by analyzing the relation between dv/v and tidal strain using
361 active source data (Yamamura et al., 2003) or noise correlation (Takano et al., 2014).
362 A similar response to crustal dilatation has also been observed during tectonic transient
363 deformation (Rivet et al., 2011). We also note that the parameter β decreases with
364 increasing lapse time (fig. 6). This lapse time evolution, combined with the depth
365 kernels (fig. 2), suggests that the long-period strain perturbations sample primarily at
366 depth (Obermann et al., 2015), rather than close to the free surface.
367   Before entering in the interpretation of this result, we will estimate the
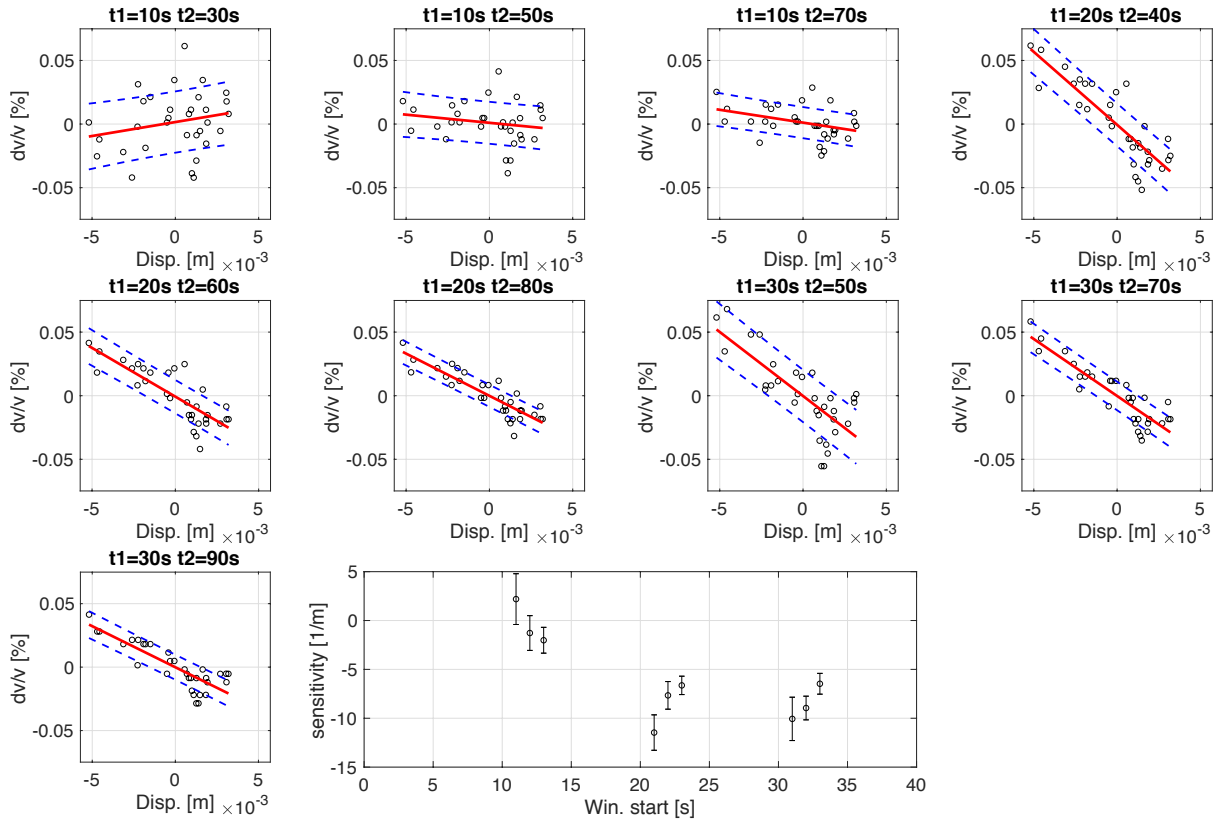368 sensitivity to co-seismic strain perturbation (sec. 4).

Figure 6: *The scatter plot represents the fit of displacement and dv/v using equation 3. The last plot is the parameter β of equation 3 as function of coda lapse time (Table 1).*

4. Estimation of sensitivity to co-seismic deformation

The study region experienced three M > 6 earthquakes during the period analyzed (2000-2017). The first is a magnitude Mw6.1 (Scognamiglio et al., 2010) occurring in 2009 near the city of L'Aquila with hypocentral depth at 8.3km. The station used to estimate the dv/v is located close (~5km) to the epicenter and experienced a peak ground velocity of 35.8cm/s (esm.mi.ingv.it). In 2016 a series of moderate-large earthquakes (Norcia-Visso sequence) struck a region ~40-70km to the north of L'Aquila. The series began on the 24 of August 2016 with a magnitude 6 followed on the 30th October 2016 by a magnitude 6.5 occurring in the same region. The last two events induced a peak ground velocity ~9cm/s (esm.mi.ingv.it). The peak ground velocity is used to calculate the dynamic strain for the mentioned earthquakes (Taira et al, 2018, assuming Vs=2500m/s), which is respectively 1.5e-4 for L'Aquila event and 4e-5 for the 24th of August event in 2016.

In concomitance with the earthquakes, large velocity drops can be observed over the full range of the analyzed lapse times (fig. 7), similar to previous observations (Zaccarelli et al., 2011, Soldati et al., 2015). Nevertheless, we here measure the values of dv/v for each time lapse and each earthquake, and we are thus able to resolve any depth dependence response of the crust to rapid dynamic perturbation induced by large earthquakes. For each event, the velocity reduction is measured as the drop from the mean dv/v over the preceding year before the events, and the following minimum peak. For the 2016 events, our analysis window (90 days) prevents us from resolving the two drops (for the 24 of August and the 30 October events respectively). We thus consider the mean reference dv/v for the year before the first event (24th of August 2016).

The co-seismic dv/v at different lapse time (Fig. 7) shows a different evolution with respect to multiyear ones (Fig. 5 and 7). For both events, we see a general reduction of dv/v as time lapse increases.
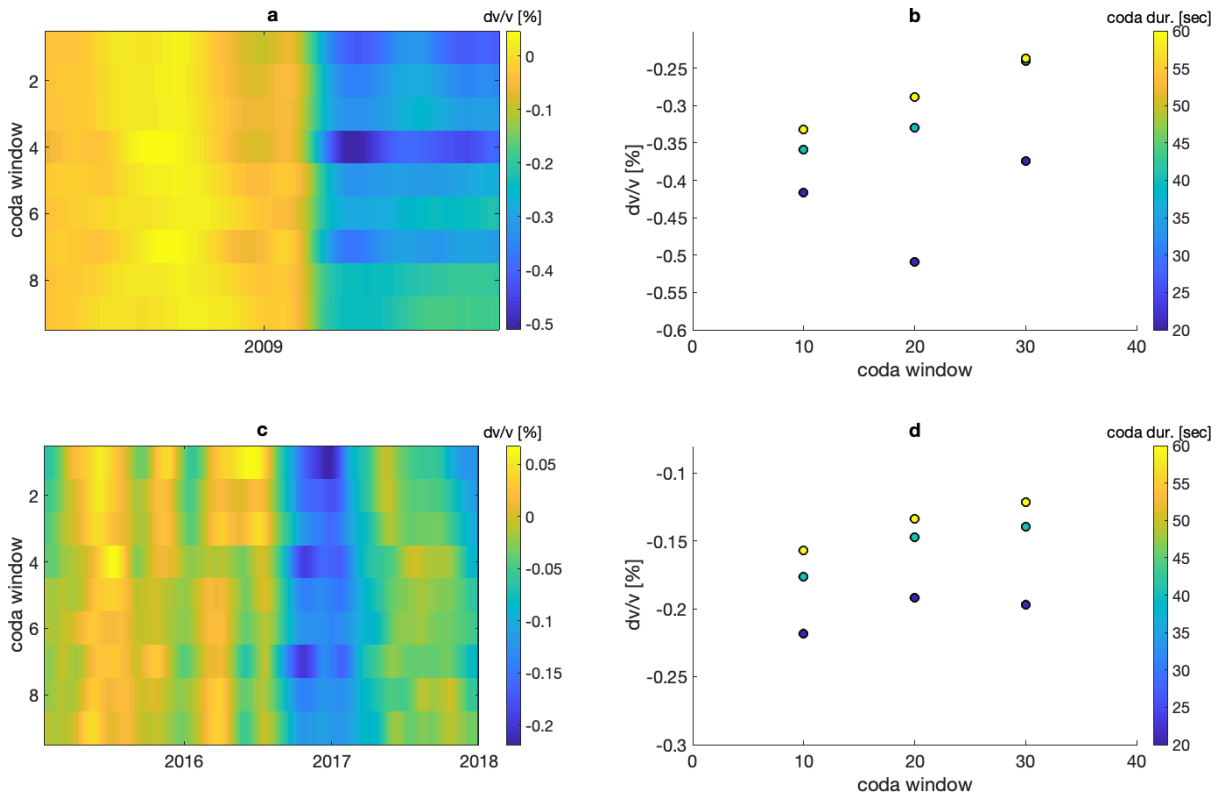
Figure 7: Coseismic dv/v time series for different lapse time (Table 1) for L'Aquila 2009 event (a) and Visso-Norcia sequence 2016 (c). Coseismic velocity reduction as function of coda lapse time (Table 1) for L'Aquila 2009 event (b) and Visso-Norcia sequence 2016 (d).

Discussion

The analysis of the 17 years of dv/v permitted us to isolate several processes controlling dv/v variations. Namely we observe velocity change due to (i) co-seismic perturbations (Fig. 7), (ii) yearly perturbations likely related to variation of temperature (Fig. 4, 5) and (iii) multi-annual perturbations associated with hydrological cycles inducing dilatational strain in the crust (Fig. 4, 5, 6, Silverii et el., 2019). By estimating dv/v over different coda lapse time (Table 1), we observe how the contribution from each process changes over different portions of the correlation coda (see Table 2, Fig. 5, 6, 7).

a. Depth resolution of velocity variations

To interpret the results for different lapse times in term of depth, we calculated the sensitivity kernel based on the single scattering 3D radiative transfer solution considering that the measured coda waves are comprised of contributions from both body and surface waves. It is important to note that, as we have no proxy to assess the coda wave constituents, this kernel can be biased. The sensitivity to surface waves is more important for early lapse times (Obermann et al., 2013). Here we assume the value of the mean free path (l = 100km and 10 km) and propagation velocity of coda waves ~ 3895 m/s, for the equipartition state. Thus, the inferred depth sensitivity is not absolute, but we can use the kernels as an indicator of the approximate depth with lapse time. The estimated sensitivity (Fig. 2) maximum is

426 approximately ~10km especially for the later coda (e.g. lapse time 20 - 50s) with 50 km
427 scattering mean free path.
428   The estimation of an absolute depth for the velocity changes will require better knowledge
429 of the scattering properties of the medium, including its layered structure, which can play a
430 fundamental role in trapping waves in some part of the medium (e.g. Kanu & Snieder, 2015).
431 Here, we can only discuss the relative depth of the velocity changes observed (multiyear,
432 seasonal, co-seismic, Fig. 5, 7) from the time lapse evolution of dv/v. For example, for multi-
433 year deformations dv/v increases for later lapse-time (Fig. 5, 7). We thus infer the existence of
434 a region at depth that exhibits sensitivity to long period forcing (Obermann et al., 2013, Hillers
435 et al., 2018). The rapid decay of the B/E ratio (eq. 2, Fig. 5b), is another indication that our late
436 coda measurements sample deeper into the crust. In fact, the thermally induced stress is
437 expected to reduce rapidly with depth (Ben-Zion & Leary, 1986) as does the ratio (Fig. 5b).

b. *Origin of various velocity variation and rheology of middle crust*

440   We begin by discussing the strain sensitivity ($e=[dv/v]/[de]$, de the dynamic strain) during
441 the co-seismic stage. Considering the dynamic strain induced by the two events we find that e
442 is respectively -1e7 and -1e8 for the L'Aquila and Amatrice earthquakes respectively. These
443 values are an order of magnitude larger than estimates in geothermal areas (Taira et al., 2018)
444 and volcanic regions (Brenguier et al., 2014), suggesting that the crustal rocks in the study
445 region are very susceptible to dynamic deformations. Under rapid perturbations induced during
446 large earthquakes the dv/v decreases with depth, suggesting significant nonlinear response
447 related to damage near the surface (e.g. Obermann, 2013, 2014), or alternatively,
448 unconsolidated granular material (e.g., Brunet et al., 2008; Johnson and Jia, 2005). For the
449 2009 event, considering the shortest analysis window in the coda (20s, Fig. 7) a peak of
450 maximum velocity reduction is observed, which suggests the existence of an isolated region at
451 depth that is highly sensitive to dynamic deformations. The detailed analysis of the co-seismic
452 response is beyond the scope of the actual work, and will be addressed in future research.
453   While the co-seismic rapid shaking induces large dv/v near the surface, the dv/v increases
454 with lapse time for the long-term perturbations (Table 2, Figure 5, 6). We interpret this time
455 lapse evolution as due to an isolated region with stronger dv/v-sensitivity to perturbations (sec.
456 a, Obermann et al., 2013, 2014, Hillers et al., 2018). While we do not have detailed evolution
457 of strain for the long-term dv/v, we can make a back-of-the-envelope calculation of the
458 sensitivity, knowing that the strain at peak GPS deformation is ~1e-6 (Silverii et al., 2019) for
459 ~1e-3 of dv/v, which gives a dv/v-sensitivity of ~1e3. This latter value agrees with other
460 estimates based on tidal-dv/v responses (Yamamura et al., 2003, Takano et al. 2014). Our
461 estimations are also in agreement with dilatant induced velocity reduction during slow slip in
462 the lower crust (Rivet et al., 2011, Wang et al., 2019).
463   Laboratory studies show that nonlinear elastic modulus variation is amplitude dependent
464 (Guyer and Johnson, 2009) as well as frequency dependent, with larger modulus changes for
465 shorter periods for a given effective pressure (Riviere et al., 2016). Here we observe a lower
466 dv/v sensitivity (1e3) for small quasi-static strain (1e-6) and low frequency (~5yrs) in contrast
467 to large dynamic strains (~1e-4) (lasting no more than few minutes) induced by the large
468 earthquakes. Under low strain forcing we also observe that non-linear material slow dynamics
469 (recovery) expressed in equation 3 is nearly zero (α, Table 2). However, for short time
470 perturbations a clear log-time recovery is observed (see for example the time after the
471 earthquakes in figure 3a). Thus, our measures reflect general behaviors of rocks in small scale
472 laboratory experiments (e.g. Riviere et al., 2016) as well as field measurements under Vibroseis
473 forcing (Johnson et al., 2008) and earthquake forcing (e.g., Brengieur et al., 2008; Wu et al.,
474 2017; Ostrovsky et al, 2019).

475   To interpret our results, we consider the velocity variation as being controlled by crack
476 density (ρ_0) because it has been well documented that cracks and other damage contribute
477 dominantly to nonlinear elastic behavior (e.g., Johnson 1998; Guyer and Johnson, 2009). The
478 sensitivity to any stress perturbations (S) can then be written as (Silver et al., 2007):
479

480
$$e = \frac{\delta v/v}{S} = \frac{\delta v/v}{\Delta \rho_0} \frac{\Delta \rho_0}{S} \quad [4]$$

481

482   As the crack density is expected to reduce with depth due to the lithostatic pressure (Tod,
483 2003), sensitivity should reduce for larger lapse time (or depth) assuming fluid pressures do
484 not vary radically. For a fixed depth dependence of strain, at shallow depth we expect larger
485 sensitivity for larger strains, as observed during the co-seismic shaking. We again note how
486 our results are anomalous for long-term deformation, as the sensitivity increases at depth (Table
487 2, Figure 5, 6). The observed dichotomy (shallow response during co-seismic forcing and
488 deeper response during long-term forcing) is similar to what has been observed in Wenchuan
489 area by Obermann et al., (2014).
490   The cause of velocity variation at late lapse time may be due to meteorological water
491 circulation in the crust. However, in this case we would expect velocity changes also at shallow
492 depth (early lapse time). Thus, alternative mechanism(s) inducing changes may exist. A
493 possibility is that forcing induced by water table variation, rather than water itself, is
494 responsible for velocity changes, with the loading (unloading) inducing significantly increment
495 (reduction) of the pore pressure and controlling the drop (increment) of velocity (Froment et
496 al., 2013, Obermann et al., 2014). This mechanism has also been observed and modeled in the
497 Irpinia region (D'Agostino et al., 2018).
498   The presence of pressurized fluids at depth a range 5-10km has been suggested by several
499 researchers for the region of L'Aquila, from analysis of earthquake source properties
500 (Tarekawa et al., 2010, Malagnini et al., 2012) or from Vp/Vs ratio (Di Luccio et al, 2012).
501 Other studies suggest an extensive dilatancy anisotropy in the central Apennines, related to
502 pervasive fluid-filled cracks oriented parallel to the Apennines chain (Pastori et al., 2016).
503 Furthermore, a significant presence of a damage zone comprised of near-fault cracks (up to
504 ~1km from the fault) are observed in the carbonate rocks near the region of L'Aquila (Agosta
505 & Aydin, 2006).
506   Putting together our results with the other geophysical information, suggests the existence
507 of a depth-isolated and long-lived (at least 9 years), intensely cracked and fluid rich, damaged
508 region in the study area. At this depth, the strong sensitivity (equation 3 and 4) is related to the
509 presence of fluids, reducing the effective pressure, thus favoring high crack density (Hamiel et
510 al., 2006) and making the material more susceptible to dynamic or quasi-static forcing.
511   Mid-crustal damage zones have been also observed in California by analysis of seismic
512 catalogs (Ben-Zion & Zaliapin, 2019). Highlighting the existence of such a damage zone is
513 fundamental as damage plays a key role in the evolution of the seismic cycle and earthquake
514 nucleation (Lyakhovsky et al., 2001, Renard et al., 2018) and controls the amount of strain
515 released in a brittle manner during the seismic cycle (Hamiel et al., 2006). For example,
516 numerical simulations show that nucleation and growth of large earthquakes is only possible
517 with the existence of a, at least modestly, damaged region (Lyakhovsky et al., 2001). Indeed,
518 Ben-Zion & Zaliapin (2019) highlighted significant damage volumes active prior to several
519 significant earthquakes in California. In a similar manner, intense seismic activity was
520 observed, concentrated near the nucleation depth of L'Aquila earthquake, in the last year
521 preceding the mainshock (e.g. Valoroso et al., 2013). Whereas seismicity solely provides a
522 volume of damage (Ben-Zion & Zaliapin, 2019), we quantitatively estimate rheological
523 parameters (e.g. sensitivity) of rocks at depth in a region of important seismic hazard.

The presence of a highly fractured rocks has implication for earthquake nucleation models. The influence of damage on a critical phase transition model has been described by Renard and others (Renard et al., 2018). In this model, cracks become more interconnected as a large event is approaching, and progressively merge into a single primary fracture (the main shock). Close to the main rupture significant precursory earthquakes must occur in the damage zone (Renard et al., 2018), similarly to what is observed in the year preceding the L'Aquila earthquake in 2009 (e.g. Valoroso et al., 2013).

We finally note (fig. 3a) how the seasonal cycle seems to disappear after the 2009 L'Aquila earthquake. Given that rain cycle remains significant after 2009, this behavior seems to suggest less sensitivity of the medium after the earthquake. However, there might exists a possible interplay between the long and slow post-seismic recovery and multiyear cycle, which will be studied in future works. Further, fluid pressures could play a key role—decreased pressures allow cracks to close and elastic non-linearity to decrease. This point needs further work.

Table 2: Summary of derived parameters

Window number	1-year cycle (eq. 2)	5 years cycle (eq. 2)	α (eq. 3)	β (eq. 3)	L'Aquila dv/v PGV=35.8cm/s Strain=1.5e-4	Amatrice dv/v PGV=9cm/s Strain=4e-5
1	*0.036*	*0.01*	*0.006*	*1.65*	*-0.39*	*-0.18*
2	0.02	0.02	0.005	-1.22	-0.34	-0.17
3	0.02	0.01	0.004	-2.22	-0.31	-0.12
4	0.02	*0.04*	*0.008*	*-11.56*	*-0.49*	-0.15
5	0.01	0.03	0.005	-7.83	-0.32	-0.11
6	0.00	0.02	0.004	-6.82	-0.28	-0.09
7	0.01	*0.04*	*0.008*	-8.79	-0.36	-0.15
8	0.00	0.03	0.005	-8.76	-0.23	-0.10
9	0.00	0.02	0.004	-6.36	-0.23	-0.08

a. Towards monitoring with seasonal loading

We showed that seasonal and multiyear components dominate the dv/v time series in the inter-seismic period (figs. 4, 5). These cycles are likely to mask smaller tectonic signals (e.g. fault weakening during earthquake preparation or transient tectonic deformations among). Indeed, systematic efforts have been applied to characterize the cyclic variations by modeling them (Wang et al. 2017) or by estimating the repeating patterns over several cycles and use their average as correction to isolate tectonic signals (Hillers et al., 2018).

Knowing the physical processes responsible for multiannual dv/v evolution (Silverii et al, 2019), we assessed the lapse time dependent response of the medium to these cycles of dilatational strain, thus turning a nuisance into an opportunity to study the crust in a region of significant seismic hazard. This approach is similar to the studies of tidal induced dv/v (Takano et al., 2014, Hillers et al., 2015b), but we here assess longer cycles, and sample deeper regions in the crust near a main active fault.

Our lapse time dv/v analysis bears similarities to laboratory dynamic nonlinear studies applied to resolve the spatial extent of damaged regions in solids (e.g., Johnson, 1998; Ulrich et al., 2007; Guyer and Johnson, 2009; Ostrovsky and Johnson, 2001; Haupert et al., 2014). As in these studies we observe a maximum response to deformation of the medium (β, eq. 3) in the damaged zone. Strain concentration can also produce highly localized increases in nonlinear response (Lott et al., 2016) especially at crack tips (e.g., Ulrich 2006), and thus time lapse monitoring could be used to reveal zones of anomalous strain accumulation.

The extension of our analysis to other regions, instrumented with dense geodetic networks and or application of InSAR allowing the accurate estimate of time-dependent strain, will help to better assess the physical properties of rocks at depth (e.g. assessing conditioning, slow

dynamics and hysteresis [Guyer and Johnson, 2009; TenCate et al., 2000]). Potential regions for new studies include New Madrid seismic zone (Craig et al., 2017) or the Himalayan region (Bettinelli et al., 2008, Bollinger et al., 2007), or Irpinia (D'Agostino et al., 2018). These regions are characterized by significant seismic risk, prominent seasonal and multiannual perturbations, and excellent seismological and geodetic instrumentation.

5. Conclusions

The precise analysis of time lapse velocity variations for 17 years of data in the region of L'Aquila permitted us to unravel the complex behavior of multiple processes controlling the dv/v evolution, over a wide range of temporal and spatial scales. The comparison of dv/v with independent measurements (e.g. dynamic strain induced by earthquakes, quasi-static strain due to hydrological cycles) permitted us to characterize the rheological response of seismogenic rocks to various level of strain at various depths. The time-lapse analysis allowed us to resolve a dichotomy in the crustal response, with significant near surface damage due to rapid strain induced by large earthquakes and deeper strain sensitivity due to long period (5yrs) and small strain perturbations in an inferred damage zone containing high fluid pressures, where the mainshock earthquake nucleates.

We showed that when the physical processes responsible for seasonal or multiyear cycles can be quantitatively characterized (e.g. Silverii et al., 2019), they can be exploited to evaluate the rheological properties of rocks in the crust. This work extends previous approaches based on tidal strain-dv/v evaluation, which are primarily sensitive to the shallowest part of the crust (<~1km, e.g. Takano et al. 2014). Furthermore, our analysis made it possible to turn hydrologically-induced cycles of dv/v, usually seen as a nuisance as they can mask tectonic events, into an opportunity to reveal the rheology of crustal rocks down to the seismogenic depth. Extending this work to other seismic active region, affected by significant weather-related cycles (Bettinelli et al., 2008, Bollinger et al., 2007, D'Agostino et al., 2018, Craig et al., 2017) will reveal new information about the physical properties of near fault rocks.

Bibliography

Agosta, Fabrizio, and Atilla Aydin. "Architecture and deformation mechanism of a basin-bounding normal fault in Mesozoic platform carbonates, central Italy." Journal of Structural Geology 28.8 (2006): 1445-1467.

Avallone, Antonio, et al. "The RING network: improvement of a GPS velocity field in the central Mediterranean." Annals of Geophysics 53.2 (2010): 39-54.

624

625 Ben-Zion, Yehuda. "Collective behavior of earthquakes and faults: Continuum‑discrete
626 transitions, progressive evolutionary changes, and different dynamic regimes." Reviews of
627 Geophysics 46.4 (2008).

628

629 Ben-Zion, Yehuda, and Peter Leary. "Thermoelastic strain in a half-space covered by
630 unconsolidated material." Bulletin of the Seismological Society of America 76.5 (1986): 1447-
631 1460.

632

633 Ben-Zion, Yehuda, and Ilya Zaliapin. "Spatial variations of rock damage production by
634 earthquakes in southern California." Earth and Planetary Science Letters 512 (2019): 184-
635 193.

636

637 Bettinelli, Pierre, et al. "Seasonal variations of seismicity and geodetic strain in the Himalaya
638 induced by surface hydrology." Earth and Planetary Science Letters 266.3-4 (2008): 332-344.

639

640 Bollinger, L., et al. "Seasonal modulation of seismicity in the Himalaya of Nepal." Geophysical
641 Research Letters 34.8 (2007).

642

643 Brenguier, F., et al. "Mapping pressurized volcanic fluids from induced crustal seismic velocity
644 drops." Science 345.6192 (2014): 80-82.

645

646 Brenguier, Florent, et al. "Postseismic relaxation along the San Andreas fault at Parkfield
647 from continuous seismological observations." science 321.5895 (2008): 1478-1481.

648

649 Brunet, T., X. Jia and P. Johnson, Transitional, elastic-nonlinear behaviour in dense granular
650 media, Geophys. Res. Lett. 35, L19308-L19311 doi:10.1029/2008GL035264 (2008).

651

652 Chiaraluce, L., et al. "The 2009 L'Aquila (Central Italy) Seismic Sequence." Bollettino di
653 Geofisica Teorica e Applicata. (2010).

654

655

656 Chiaraluce, L., et al. "The anatomy of the 2009 L'Aquila normal fault system (central Italy)
657 imaged by high resolution foreshock and aftershock locations." Journal of Geophysical
658 Research: Solid Earth 116.B12 (2011).

659

660 Craig, Timothy J., Kristel Chanard, and Eric Calais. "Hydrologically-driven crustal stresses
661 and seismicity in the New Madrid Seismic Zone." Nature communications 8.1 (2017): 2143.

662

663 Chiaraluce, Lauro, et al. "The 2016 central Italy seismic sequence: A first look at the
664 mainshocks, aftershocks, and source models." Seismological Research Letters 88.3 (2017):
665 757-771.

666

667 Chiaraluce, L. "Unravelling the complexity of Apenninic extensional fault systems: a review of
668 the 2009 L'Aquila earthquake (Central Apennines, Italy)." Journal of Structural Geology 42
669 (2012): 2-18.

670

671 D'Agostino, N. "Complete seismic release of tectonic strain and earthquake recurrence in the
672 Apennines (Italy)." Geophysical Research Letters 41.4 (2014): 1155-1162.

673

D'Agostino, Nicola, et al. "Crustal deformation and seismicity modulated by groundwater recharge of karst aquifers." Geophysical Research Letters 45.22 (2018): 12-253.

Delorey, Andrew A., Nicholas J. van der Elst, and Paul A. Johnson. "Tidal triggering of earthquakes suggests poroelastic behavior on the San Andreas Fault." Earth and Planetary Science Letters 460 (2017): 164-170.

Di Luccio, F., et al. "Normal faults and thrusts reactivated by deep fluids: The 6 April 2009 Mw 6.3 L'Aquila earthquake, central Italy." Journal of Geophysical Research: Solid Earth 115.B6 (2010).

Froment, B., et al. "Deformation at depth associated with the 12 May 2008 Mw 7.9 Wenchuan earthquake from seismic ambient noise monitoring." Geophysical Research Letters 40.1 (2013): 78-82.

Guyer, Robert A., and Paul A. Johnson. "Nonlinear mesoscopic elasticity: Evidence for a new class of materials." Physics today 52 (1999): 30-36.

Guyer, Robert A., and Paul A. Johnson. Nonlinear mesoscopic elasticity: the complex behaviour of rocks, soil, concrete. John Wiley & Sons, 2009.

Hamiel, Yariv, et al. "Stable and unstable damage evolution in rocks with implications to fracturing of granite." Geophysical Journal International 167.2 (2006): 1005-1016.

Herrmann, R. B. (2013). Computer programs in seismology: An evolving tool for instruction and research. Seismological Research Letters,
84(6), 1081–1088. https://doi.org/10.1785/0220110096

Haupert, Sylvain, et al. "Optimized dynamic acousto-elasticity applied to fatigue damage and stress corrosion cracking." Journal of Nondestructive Evaluation 33.2 (2014): 226-238.

Hillers, G., et al. "Seasonal variations of seismic velocities in the San Jacinto fault area observed with ambient seismic noise." Geophysical Journal International 202.2 (2015a): 920-932.

Hillers, G., et al. "In situ observations of velocity changes in response to tidal deformation from analysis of the high-frequency ambient wavefield." Journal of Geophysical Research: Solid Earth 120.1 (2015b): 210-225.

Hillers, Gregor, et al. "Transient change of seismic velocities in the San Jacinto fault region following the 2010 M7. 2 El Mayor-Cucapah earthquake observed with ambient noise monitoring." EGU General Assembly Conference Abstracts. Vol. 20. 2018.

Johnson, P. A. and X. Jia, Nonlinear dynamics, granular media and dynamic earthquake triggering, Nature, 473 871-874 (2005)

Johnson, P., Robert Guyer, and L. Ostrovsky. A nonlinear mesoscopic elastic class of materials. No. LA-UR-99-4733. Los Alamos National Lab., NM (US), 1999.

724 *Johnson, Paul A. "The new wave in acoustic testing." Materials World (1999): 544-546.*

726 *Johnson, Paul A., et al. "Inducing in situ, nonlinear soil response applying an active*
727 *source." Journal of Geophysical Research: Solid Earth 114.B5 (2009).*

729 *Kanu, Chinaemerem, and Roel Snieder. "Numerical computation of the sensitivity kernel for*
730 *monitoring weak changes with multiply scattered acoustic waves." Geophysical Supplements*
731 *to the Monthly Notices of the Royal Astronomical Society 203.3 (2015): 1923-1936.*

733 *Lacombe, Céline, et al. "Separation of intrinsic absorption and scattering attenuation from*
734 *Lg coda decay in central France using acoustic radiative transfer theory." Geophysical*
735 *Journal International 154.2 (2003): 417-425.*

737 *L.D. Landau & E.M. Lifshitz Theory of Elasticity (Volume 7 of A Course of Theoretical*
738 *Physics) Pergamon Press 1970*

740 *Lobkis, O. I., and R. L. Weaver (2003), Coda-wave interferometry in finite solids: Recovery of*
741 *P-to-S conversion rates in an elastodynamic billiard, Phys. Rev. Lett., 90(25), 254302,*
742 *doi:10.1103/PhysRevLett.90.254302.*

744 *Lott, Martin, et al. "From local to global measurements of nonclassical nonlinear elastic*
745 *effects in geomaterials." The Journal of the Acoustical Society of America 140.3 (2016):*
746 *EL231-EL235.*

747 *Lott, Martin, et al. "Three-dimensional modeling and numerical predictions of multimodal*
748 *nonlinear behavior in damaged concrete blocks." The Journal of the Acoustical Society of*
749 *America 144.3 (2018): 1154-1159.*

750 *Lyakhovsky, V., Ben-Zion, Y., Agnon, A., 2001. Earthquake cycle, fault zones, and seismicity*
751 *patterns in a rheologically layered lithosphere. J. Geophys. Res. 106, 4103–4120.*

752 *Malagnini, Luca, et al. "Control of pore fluid pressure diffusion on fault failure mode: Insights*
753 *from the 2009 L'Aquila seismic sequence." Journal of Geophysical Research: Solid*
754 *Earth 117.B5 (2012).*

756 *Margerin, Ludovic, Michel Campillo, and Bart Van Tiggelen. "Monte Carlo simulation of*
757 *multiple scattering of elastic waves." Journal of Geophysical Research: Solid Earth 105.B4*
758 *(2000): 7873-7892.*

760 *McCall, K. R., and R. A. Guyer. Hysteresis and nonlinear elasticity in rocks. No. LA-UR-93-*
761 *4143; CONF-9308167-5. Los Alamos National Lab., NM (United States), 1993.*

763 *Obermann, Anne, et al. "Depth sensitivity of seismic coda waves to velocity perturbations in*
764 *an elastic heterogeneous medium." Geophysical Journal International 194.1 (2013): 372-382.*

766 *Obermann, Anne, et al. "Seismic noise correlations to image structural and mechanical*
767 *changes associated with the Mw 7.9 2008 Wenchuan earthquake." Journal of Geophysical*
768 *Research: Solid Earth 119.4 (2014): 3155-3168.*

Ostrovsky, L. A., and P. A. Johnson. "Dynamic nonlinear elasticity in geo materials." Rivista del Nuovo Cimento della Societa Italiana di Fisica 24.7 (2001): 1-46.

Ostrovsky, Lev, et al. "Long-Time Relaxation Induced by Dynamic Forcing in Geomaterials." Journal of Geophysical Research: Solid Earth (2019).

Pacheco, Carlos, and Roel Snieder. "Time-lapse travel time change of multiply scattered acoustic waves." The Journal of the Acoustical Society of America 118.3 (2005): 1300-1310.

Paasschens, J. C. J. "Solution of the time-dependent Boltzmann equation." Physical Review E 56.1 (1997): 1135.

Pastori, Marina, Paola Baccheschi, and Lucia Margheriti. "Shear wave splitting evidence and relations with stress field and major faults from the "Amatrice-Visso-Norcia Seismic Sequence"." Tectonics (2019).

Planès, Thomas, et al. "Decorrelation and phase-shift of coda waves induced by local changes: multiple scattering approach and numerical validation." Waves in Random and Complex Media 24.2 (2014): 99-125.

Poli, P., et al. "Noise directivity and group velocity tomography in a region with small velocity contrasts: the northern Baltic shield." Geophysical Journal International 192.1 (2012): 413-424.

Poupinet, G., W. Ellsworth, and J. Frechet (1984), Monitoring velocity variations in the crust using earthquake doublets: An application to the Calaveras Fault, California, J. Geophys. Res., 89(B7), 5719–5731.

Renard, F., Weiss, J., Mathiesen, J., Ben Zion, Y., Kandula, N., Cordonnier, B., 2018. Critical evolution of damage towards system-size failure in crystalline rock. J. Geophys. Res. 123, 1969–1986. https://doi.org/10.1002/2017JB014964.

Renaud, Guillaume, Samuel Callé, and Marielle Defontaine. "Remote dynamic acoustoelastic testing: Elastic and dissipative acoustic nonlinearities measured under hydrostatic tension and compression." Applied Physics Letters 94.1 (2009): 011905.

Renaud, G., P-Y. Le Bas, and P. A. Johnson. "Revealing highly complex elastic nonlinear (anelastic) behavior of Earth materials applying a new probe: Dynamic acoustoelastic testing." Journal of Geophysical Research: Solid Earth 117.B6 (2012).

Richter, Tom, et al. "Comprehensive observation and modeling of earthquake and temperature-related seismic velocity changes in northern Chile with passive image interferometry." Journal of Geophysical Research: Solid Earth 119.6 (2014): 4747-4765.

Rivet, Diane, et al. "Seismic evidence of nonlinear crustal deformation during a large slow slip event in Mexico." Geophysical Research Letters 38.8 (2011).

Rivière, J., L. Pimienta, M. Scuderi, T. Candela, P. Shokouhi, J. Fortin, A. Schubnel, C. Marone, and P. A. Johnson (2016), Frequency, pressure, and strain dependence of nonlinear elasticity in Berea Sandstone, Geophys. Res. Lett., 43, 3226–3236, doi:10.1002/2016GL068061.

818 *Rivière, Jacques & Shokouhi, Parisa & Guyer, Robert & Johnson, Paul. (2015). A set of*
819 *measures for the systematic classification of the nonlinear elastic behavior of disparate rocks.*
820 *Journal of Geophysical Research: Solid Earth. 120. 10.1002/2014JB011718.*
821
822 *Sabra, Karim G., et al. "Extracting time-domain Green's function estimates from ambient*
823 *seismic noise." Geophysical Research Letters 32.3 (2005).*
824
825 Scognamiglio, L., Tinti, E., Quintiliani, M. (2006). Time Domain Moment Tensor [Data set]. Istituto
826 Nazionale di Geofisica e Vulcanologia (INGV). https://doi.org/10.13127/TDMT
827
828 *Scognamiglio, Laura, et al. "Fast determination of moment tensors and rupture history: What*
829 *has been learned from the 6 April 2009 L'Aquila earthquake sequence." Seismological*
830 *Research Letters 81.6 (2010): 892-906.*
831
832 *Sens-Schönfelder, Christoph, Roel Snieder, and Xun Li. "A model for nonlinear elasticity in*
833 *rocks based on friction of internal interfaces and contact aging." Geophysical Journal*
834 *International216.1 (2018): 319-331.*
835
836 *Soldati, Gaia, et al. "Monitoring of crustal seismic velocity variations in the L'Aquila fault*
837 *zone inferred from noise cross-correlation." Geophysical Journal International 202.1 (2015):*
838 *604-611.*
839
840 *Shapiro, Nikolai M., and Michel Campillo. "Emergence of broadband Rayleigh waves from*
841 *correlations of the ambient seismic noise." Geophysical Research Letters 31.7 (2004).*
842
843 *Silver, Paul G., et al. "Active source monitoring of cross-well seismic travel time for stress-*
844 *induced changes." Bulletin of the Seismological Society of America 97.1B (2007): 281-293.*
845
846 *Silverii, Francesca, et al. "Transient deformation of karst aquifers due to seasonal and*
847 *multiyear groundwater variations observed by GPS in southern Apennines (Italy)." Journal of*
848 *Geophysical Research: Solid Earth 121.11 (2016): 8315-8337.*
849
850 *Silverii, Francesca, et al. "Transient crustal deformation from karst aquifers hydrology in the*
851 *Apennines (Italy)." Earth and Planetary Science Letters 506 (2019): 23-37.*
852
853 *TenCate, J.A., E. Smith, and R.t A. Guyer, Universal Slow Dynamics in Granular Solids. Phys.*
854 *Rev. Lett. 85, 1020 (2000)*
855
856 *Van Den Abeele, Koen & Visscher, Joëlle. (2000). Damage Assessment in reinforced concrete*
857 *using spectral and temporal nonlinear vibration techniques. Cement and Concrete Research.*
858 *30. 1453-1464. 10.1016/S0008-8846(00)00329-X.*
859
860 *van der Elst, Nicholas J., et al. "Fortnightly modulation of San Andreas tremor and low-*
861 *frequency earthquakes." Proceedings of the National Academy of Sciences 113.31 (2016):*
862 *8601-8605.*
863
864 Valoroso, L., et al. "Radiography of a normal fault system by 64,000 high-precision earthquake
865 locations: The 2009 L'Aquila (central Italy) case study." *Journal of Geophysical Research:*
866 *Solid Earth* 118.3 (2013): 1156-1176.
867

Weaver, Richard L. "On diffuse waves in solid media." The Journal of the Acoustical Society of America 71.6 (1982): 1608-1609.

Yamamura, Keiko, et al. "Long-term observation of in situ seismic velocity and attenuation." Journal of Geophysical Research: Solid Earth 108.B6 (2003).

Taira, Taka'aki, et al. "Monitoring reservoir response to earthquakes and fluid extraction, Salton Sea geothermal field, California." Science Advances 4.1 (2018): e1701536.

Takano, Tomoya, et al. "Seismic velocity changes caused by the Earth tide: Ambient noise correlation analyses of small-array data." Geophysical Research Letters 41.17 (2014): 6131-6136.

Terakawa, Toshiko, et al. "High-pressure fluid at hypocentral depths in the L'Aquila region inferred from earthquake focal mechanisms." Geology 38.11 (2010): 995-998.

Tod, S. R. "Bed-limited cracks in effective medium theory." Geophysical Journal International 152.2 (2003): 344-352.

Ulrich, T. J., P. A. Johnson, and R. A. Guyer, Interaction Dynamics of Elastic Waves with a Complex Nonlinear Scatterer through the Use of a Time Reversal Mirror, Phys. Rev. Lett. 98, 104301 (2007).

Wang, Qing-Yu, et al. "Seasonal crustal seismic velocity changes throughout Japan." Journal of Geophysical Research: Solid Earth122.10 (2017): 7987-8002.

Wang, Qing-Yu, et al. "Evidence of changes of seismic properties in the entire crust beneath Japan after the Mw 9.0, 2011 Tohoku-oki earthquake." Journal of Geophysical Research: Solid Earth (2019).

Wu, Chunquan, et al. "Constraining depth range of S wave velocity decrease after large earthquakes near Parkfield, California." Geophysical Research Letters 43.12 (2016): 6129-6136.

Zaccarelli, Lucia, et al. "Variations of crustal elastic properties during the 2009 L'Aquila earthquake inferred from cross-correlations of ambient seismic noise." Geophysical Research Letters 38.24 (2011).